LETTER

An absorption-based approach to improved estimates of phytoplankton biomass and net primary production

James Fox [ORCID],[1]* Sasha J. Kramer,[2] Jason R. Graff,[3] Michael J. Behrenfeld,[3] Emmanuel Boss [ORCID],[4] Gavin Tilstone,[5] Kimberly H. Halsey[1]

[1]Department of Microbiology, Oregon State University, Corvallis, Oregon; [2]Interdepartmental Graduate Program in Marine Science, University of California, Santa Barbara, Santa Barbara, California; [3]Department of Botany and Plant Pathology, Oregon State University, Corvallis, Oregon; [4]School of Marine Sciences, University of Maine, Orono, Maine; [5]Plymouth Marine Laboratory, Plymouth, UK

Scientific Significance Statement

Estimates of phytoplankton biomass are essential components of primary production models and are also required for the calculation of other useful model outputs that provide insight into nutrient cycling and carbon transfer through marine food webs. Optical proxies provide observations of phytoplankton carbon at unparalleled spatial and temporal resolution but require scaling factors that have not captured variability driven by changes in community composition or physiology. Here, we describe a new approach that improves model estimates of net primary production by mechanistically scaling optical measurements to phytoplankton carbon in a way that accounts for variation in taxonomy.

Abstract

The abundance and productivity of phytoplankton constrain energy transfer through marine food webs and the export of organic carbon to the deep ocean. Bio-optical measurements correlate well with phytoplankton carbon (C_{phyto}), but the effect of taxonomic variability on this relationship is still uncertain. Here, we explore how changes in phytoplankton community composition influence the relationship between the particulate backscatter coefficient (b_{bp}) and C_{phyto} and present a new approach to estimate phytoplankton biomass more accurately using b_{bp}. We found that using a fixed scaling factor for the conversion of b_{bp} to C_{phyto} could lead to the underestimation or overestimation of biomass, depending on the dominant taxonomic group in the phytoplankton community. In addition, we demonstrate how a simple ratio of absorption at two wavelengths can be used to provide a coarse approximation of phytoplankton community composition when scaling b_{bp} to C_{phyto}, thereby improving the estimation of net primary production.

The abundance and taxonomic composition of marine phytoplankton fundamentally impact the fate of organic carbon fixed through net primary production (NPP). Environmental conditions such as light, nutrient availability, turbulence, and grazing ultimately determine phytoplankton community structure, food web dynamics, and elemental cycling. Cyanobacteria typically dominate (both numerically and as a fraction of biomass) stratified oligotrophic systems that are often associated with rapid carbon cycling driven by the microbial loop (Marañón et al. 2003; Flombaum et al. 2013). Diatoms are another taxonomic group that are widely distributed in the surface ocean (Kemp and Villareal 2018). When growth conditions in the mixed layer are improving and if nutrient levels are sufficient, the growth rate of diatoms can become temporally decoupled from grazing pressure and a large diatom-dominated bloom can occur (Behrenfeld et al. 2021). These decoupling events sometimes result in high magnitude carbon export events that can include large aggregates of cells, but this is not always the case (Martin et al. 2011; Durkin et al. 2016). As global change alters the physical and chemical nature of the ocean, it will give rise to shifts in the abundance and composition of phytoplankton communities and their role in biogeochemical cycles (Finkel et al. 2010; Henson et al. 2019).

Primary production is the product of phytoplankton growth rate and carbon biomass, but few direct measurements of phytoplankton carbon (C_{phyto}) exist due to the complex methods required to isolate phytoplankton cells from other components of the particulate organic carbon (POC) pool (Graff et al. 2012). Particulate backscattering (b_{bp}) correlates well with analytical measurements of C_{phyto} and can also be estimated using satellite remote sensing, thereby allowing the assessment of phytoplankton biomass distribution at a global scale (Behrenfeld et al. 2005; Graff et al. 2015; Martínez-Vicente et al. 2017). After correcting for the background influence of non-algal particles, b_{bp} is converted to C_{phyto} using a scaling factor determined from in situ measurements (Martinez-Vicente et al. 2013; Graff et al. 2015). Multiple scaling factors have been recommended and range in magnitude by twofold (Behrenfeld et al. 2005; Martinez-Vicente et al. 2013; Graff et al. 2015), but the factors impacting the empirical relationship between b_{bp} and C_{phyto} (e.g., phytoplankton taxonomy and size) have not yet been critically evaluated over large spatial scales (Qiu et al. 2021). Here, we employ a new absorption-based method that accounts for taxonomic variability when scaling b_{bp} to C_{phyto}. The new method improves estimates of NPP and can be used to coarsely evaluate phytoplankton community composition across time and space.

Methods

Data from the North Atlantic Aerosol and Marine Ecosystem Study (NAAMES; Chase et al. 2020), the EXport Processes in the Ocean from RemoTe Sensing program (EXPORTS; Siegel
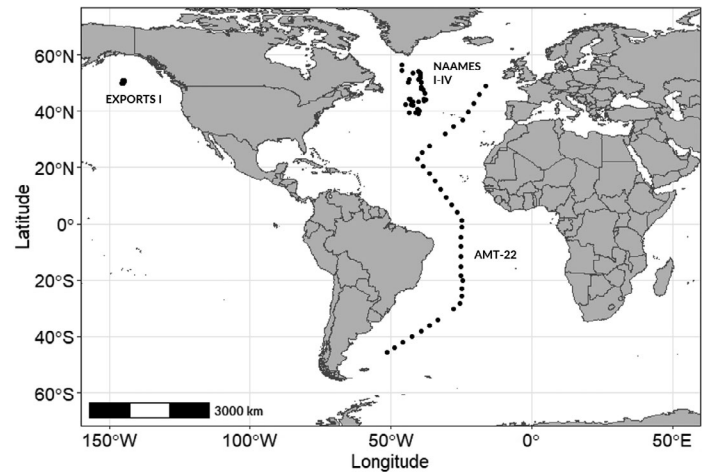
Fig. 1. Cruise tracks for the NAAMES field campaigns, the EXPORTS program in the North Pacific, and AMT22.

et al. 2021), and the 22nd Atlantic Meridional Transect (AMT22; Graff et al. 2015) were analyzed to investigate how phytoplankton community composition influences the relationship between bio-optical measurements and biomass (Fig. 1). The collective dataset includes near-surface optical properties acquired from semi-continuous inline sampling of the ship's underway water supply, which were used to provide effective proxies for key biological parameters, and discrete samples collected for high-performance liquid chromatography (HPLC) phytoplankton pigments and flow cytometry. Although a brief overview of methods and protocols is provided below, more details on modeled parameters and instrumentation are provided in the supplemental information.

Chlorophyll and POC

Estimates of chlorophyll concentration were derived from the phytoplankton absorption coefficient (a_ϕ) at 676 nm using particulate absorption [$a_p(\lambda)$] red peak line height as in Boss et al. (2007; Eq. 1).

$$a_\phi(676) = [a_p(676) - 39/65 a_p(650) - 26/65 a_p(715)]. \quad (1)$$

For each cruise, values of $a_\phi(676)$ were then calibrated against chlorophyll a concentrations measured by HPLC to provide a proxy for chlorophyll (Chl_{ACS}) specific to each region as in Boss et al. (2013). POC was estimated using particulate beam attenuation at 660 nm, $c_p(660)$, and scaling coefficients specific to the AMT22 cruise calculated in Fig. 5c of Graff et al. (2015; Eq. 2). The AMT22 values are similar to global and regional coefficients previously calculated for the North Atlantic and South Atlantic (Gardner et al. 2006; Cetinić et al. 2012).

$$POC = c_p(660) \cdot 420 + 6.4. \quad (2)$$

Phytoplankton carbon

Multiple approaches were used to calculate C_{phyto}. The first approach followed the methods of Graff et al. (2015), which calculates phytoplankton biomass using a scaled value of the particulate backscatter coefficient at 470 nm [$b_{bp}(470)$], here we refer to these values as $C_{b_{bp}}$:

$$C_{b_{bp}} = b_{bp}(470) \cdot 12,128 + 0.59. \quad (3)$$

In a second approach, modeled phytoplankton carbon (C_{mod}) values were calculated using Chl_{ACS}, photosynthetically active radiation (PAR), the light attenuation coefficient (K_d), and the median growth irradiance in the surface mixed layer (I_g) as described in Fox et al. (2020):

$$C_{mod} = \left(19 \cdot e^{\left(0.038 \cdot \frac{PAR^{0.45}}{K_d} \right)} \cdot \frac{1 + e^{(-0.15 \cdot PAR)}}{1 + e^{(-3 \cdot I_g)}} \right) \cdot Chl_{ACS}. \quad (4)$$

Hyperspectral measurements of the absorption spectrum were used to develop a simple method for scaling b_{bp} to C_{phyto} that accounts for taxonomic variability. Total non-water particulate absorption, $a_{nw}(\lambda)$, measurements across the visible spectrum (400–700 nm) were averaged at 5 nm increments between 400 and 700 nm. A two-wavelength ratio matrix was then created for all available wavelengths before Pearson correlation coefficients and Type II linear regression were used to compare each ratio to model-based scaling factor [$SF_{mod} = C_{mod}/b_{bp}(470)$] values determined a priori using estimates of $b_{bp}(470)$ and C_{mod} (Fig. 2; Supporting Information Fig. S1). Comparative analyses between phytoplankton absorption ratios and SF_{mod} showed the best correlation with the $a_{nw}(690\,nm)/a_{nw}(580\,nm)$ ratio ($r^2 = 0.56$, Root Mean
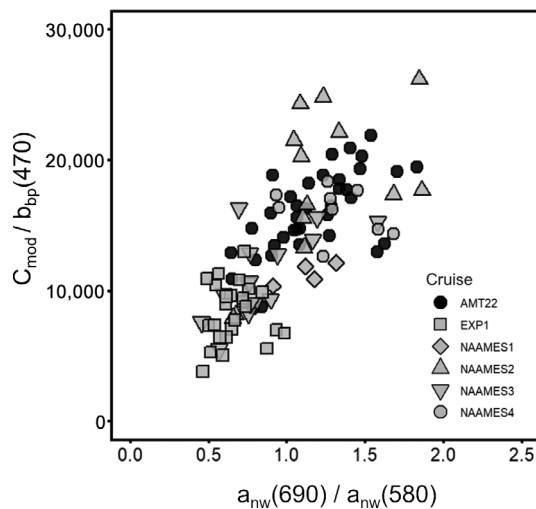
Fig. 2. Scaling factors determined using modeled carbon, C_{mod}, and the particulate backscatter coefficient at 470 nm, $b_{bp}(470)$, compared with the ratio of phytoplankton absorption at 690 and 580 nm [$y = (12,287)x$, $r^2 = 0.56$, RMSE = 3512]. Symbol shape and fill indicate the research cruise.

Square Error = 3512, scalar units = mg C m^{-3}; Fig. 2). This ratio was used to derive a variable scaling factor to estimate phytoplankton biomass (C_{var}, Eq. 5):

$$C_{var} = \left[(b_{bp}(470) - 0.00027) \cdot \left(\frac{a_{nw}(690)}{a_{nw}(580)} \cdot 12287 \right) \right]. \quad (5)$$

Here, C_{var} was estimated using b_{bp} after subtracting the "background" value of 0.00027 m^{-1} before multiplying by the scaling factor of 12,287 that varies with the absorbance ratio. The "background" component was calculated using the slope and x-axis intercept from regression analysis of the bulk community C_{mod}–b_{bp} relationship (Supporting Information Fig. S2) and is consistent with similar estimates made using satellite or in situ data (i.e., 0.00027 m^{-1} for this study compared to a value of 0.00035 m^{-1} determined from remotely sensed b_{bp} vs. chl; Behrenfeld et al. 2005) and values of 0.00058 and 0.00067 m^{-1} derived from flow-cytometric cell volume-based estimates of carbon and b_{bp} (Martinez-Vicente et al. 2013; Qiu et al. 2021). The value of 12,287 was taken from the slope of the regression analysis between C_{mod} and $\frac{a_{nw}(690)}{a_{nw}(580)}$ (Fig. 2).

Finally, phytoplankton carbon measurements derived from flow cytometry (C_{fcm}) were calculated using group-specific abundance and biovolume data (Graff et al. 2015). Values for the group-specific diameter estimates and biovolume-carbon conversions were taken from previous studies from the AMT program (Heywood et al. 2006; Tarran et al. 2006; Martinez-Vicente et al. 2013).

Phytoplankton taxonomy

A network-based community detection analysis was used to determine the dominant pigment-based phytoplankton groups in the community following Kramer et al. (2020). Five distinguishable groups were determined and combined into three populations roughly based on cell size: (1) cyanobacteria and haptophytes (pico-nano), (2) green algae/mixed (pico-nano), (3) diatoms and dinoflagellates (nano-micro).

Phytoplankton growth and productivity

Phytoplankton growth rate (μ) was modeled using near-surface optical measurements of Chl_{ACS}, PAR, mixed layer depth (MLD), and K_d (see Supporting Information Methods). NPP was estimated as the product of the resultant growth rates and the three different C_{phyto} estimates (e.g., C_{mod}, $C_{b_{bp}}$, and C_{var}) (Eq. 6).

$$NPP = \mu \cdot C_{phyto}. \quad (6)$$

Model-based NPP was compared to discrete measurements determined using ^{14}C uptake incubations ranging between 10 and 24 h in duration (Tilstone et al. 2009; Fox et al. 2020; Siegel et al. 2021).

The code, data, and metadata of this study are available in the Zenodo data repository (Fox et al. 2022).

Results

### Scaling particulate backscatter to phytoplankton carbon

Surface measurements of $b_{bp}(470)$ and C_{mod} correlated well for the bulk plankton community ($r^2 = 0.76$, RMSE = 10.1 mgC m^{-3}, $n = 124$; Supporting Information Fig. S2), but regression analysis showed that the scaling factor used to convert b_{bp} to C_{mod} ranges from 3770 to 27,697 and is influenced by taxonomy (Fig. 3). For phytoplankton populations dominated by green algae, the scalar was 13,832 ± 1142 mg C m^{-3} (i.e., $C_{mod} = b_{bp} \times 13{,}832$), which is similar to previous estimates of 13,000 by Behrenfeld et al. (2005) and 12,128 by Graff et al. (2015). However, the scalars best fitting the diatom/dinoflagellate and cyanobacteria/haptophytes communities were 22,641 ± 1714 and 8372 ± 670, respectively, suggesting that the use of a fixed scaling factor leads to under- or overestimates of C_{phyto}. Accounting for taxonomic variability in this relationship will therefore yield a more accurate conversion from b_{bp}.

### Latitudinal changes in phytoplankton carbon and contribution to total POC

The accuracy of the C_{var} estimates was assessed using near-surface bio-optical estimates of phytoplankton carbon measured by flow cytometry (C_{fcm}) during AMT22. Estimates of C_{var} closely matched estimates of C_{fcm} over a broad latitudinal gradient north of 35°S ($r^2 = 0.79$, RMSE = 1.70 mgC m^{-3}; Supporting Information Fig. S3a) and captured a greater amount of the variability observed in the C_{fcm} data than $C_{b_{bp}}$ estimated using a fixed scaling factor ($r^2 = 0.46$, RMSE = 1.14 mgC m^{-3}; Fig. 4a).

Optically-derived POC was used to evaluate the contribution of phytoplankton carbon to the total POC pool over the AMT22 track. C_{var} : POC estimates generally matched well with C_{fcm} : POC in latitudes north of 35°S ($r^2 = 0.69$, RMSE = 0.05; Supporting Information Fig. S3b), but the relationship deteriorated in more southerly regions (Fig. 4b; Supporting Information Fig. S3d). In the northerly latitudes, the C_{var} : POC relationship was largely driven by changes in the abundance of *Synechococcus* spp. and *Prochlorococcus* spp., which often contributed over 80% of the total C_{fcm}. Values of C_{var} effectively tracked changes in picocyanobacterial biomass, while the fixed scalar approach generally led to estimates higher than those of C_{fcm} in areas dominated by picocyanobacteria and showed little spatial change north of 35°S. As a result, $C_{b_{bp}}$: POC remained relatively consistent
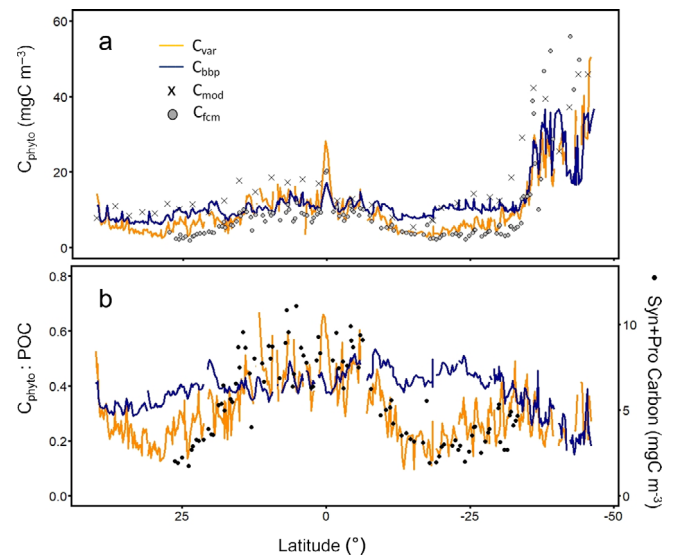
Fig. 4. Latitudinal trends in surface (**a**) phytoplankton carbon estimated using $b_{bp}(470)$ scaled using a variable (C_{var}, orange line) and fixed ($C_{b_{bp}}$, blue line) scaling factor, flow cytometry (C_{fcm}, gray circles) and a model (C_{mod}, black crosses), and (**b**) phytoplankton carbon-to-POC ratios calculated using C_{var} (orange line) and $C_{b_{bp}}$ (blue line) during AMT22. Black circles are the total carbon of *Synechococcus* spp. and *Prochlorococcus* spp. when they contribute over 80% of the total biomass estimated by flow cytometry.
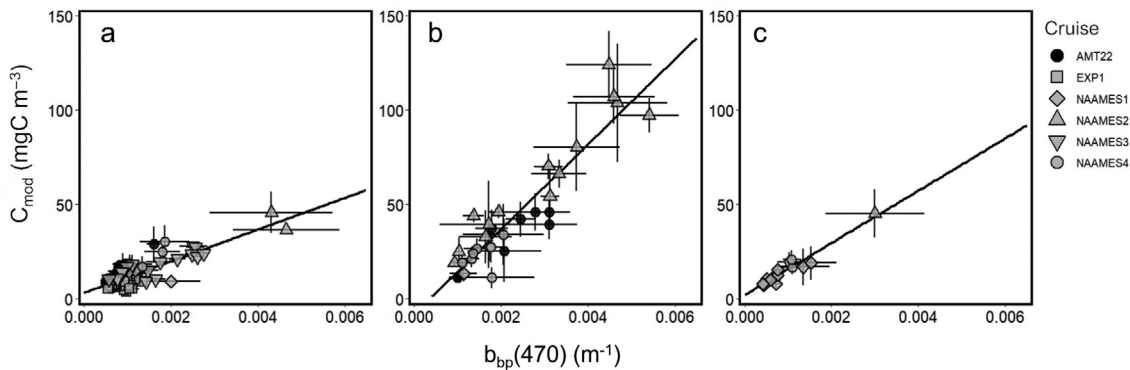
Fig. 3. Modeled phytoplankton carbon, C_{mod}, and measurements of the particulate backscatter coefficient at 470 nm, $b_{bp}(470)$, for (**a**) cyanobacteria and haptophyte populations ($r^2 = 0.65$, RMSE = 4.5, $y = (8372)x + 3.3$); (**b**) diatoms and dinoflagellates populations ($r^2 = 0.85$, RMSE = 11.7, $y = (22{,}495)x - 8.0$); and (**c**) green algae or mixed populations ($r^2 = 0.92$, RMSE = 2.74, $y = (13{,}832)x + 2.0$). Solid line is the linear fit for each taxonomic grouping. Points are daily means, error bars are standard deviation. Symbol shape and fill indicates which research cruise data were collected.

to 35°S. South of this latitude, *Synechococcus* spp. and *Prochlorococcus* spp. decreased substantially in their relative contributions to total phytoplankton biomass (Fig. 4). The magnitude and spatial variability observed in the C_{var} to POC relationship closely match trends observed in previous AMT campaigns (Martinez-Vicente et al. 2013; Graff et al. 2015).

### Modeled primary production across diverse ecosystems

The above analysis implies that estimates of NPP modeled over a wide range of ecosystem states and conditions are improved by using biomass values calculated using a variable scaling factor (C_{var}) compared to a fixed scaling factor ($C_{b_{bp}}$) (Fig. 5; Table 1). This result is most notable for the NAAMES 3 and AMT22 cruises, which sampled predominantly in oligotrophic waters where the phytoplankton communities were dominated by cyanobacteria. All approaches used to estimate C_{phyto} performed similarly in high biomass/high productivity conditions, but C_{var} showed modest improvements over $C_{b_{bp}}$ at two stations during NAAMES 2 (Fig. 5b,c). The second NAAMES cruise took place during the climax of the spring bloom when the phytoplankton community was dominated by eukaryotic phytoplankton, and small diatoms were prevalent at the two stations where the NPP estimates were most improved (Bolaños et al. 2020). Model estimates were typically higher than ^{14}C estimates of NPP, which could be due to subsurface light levels being overestimated because of an underestimate in K_d (Xing and Boss 2021).

Discussion and conclusions

The overarching objectives of this study were to assess the impact of community composition on in situ b_{bp}-based estimates of phytoplankton biomass and to develop a new method that improves C_{phyto} estimates by accounting for taxonomic variability in the phytoplankton community. While a relationship between b_{bp} and C_{phyto} is well established

(Behrenfeld et al. 2005; Martinez-Vicente et al. 2013; Graff et al. 2015), we found that community composition can significantly impact the magnitude of the scaling factor required in these calculations, which is consistent with previous observations in the oligotrophic South China Sea (Qiu et al. 2021). For populations dominated by cyanobacteria or haptophytes, our estimated scaling factor was 25% to 30% lower than the fixed values currently applied to scale in situ or satellite retrievals of b_{bp} to C_{phyto}. The fixed scalars likely result in systematic overestimations of C_{phyto} when employed in areas dominated by picocyanobacteria, such as the permanently stratified gyres and seasonally oligotrophic regions. Conversely, the scalar best fitting diatom and dinoflagellate populations was almost 100% larger than some fixed scalar estimates (Behrenfeld et al. 2005; Graff et al. 2015). Thus, use of a fixed scalar will typically underestimate C_{phyto} when these phytoplankton groups are dominant, especially during high biomass bloom events. The need for alternative scaling factors could explain previously reported inaccuracies in NPP modeled using b_{bp}, where predicted values in the western North Atlantic were higher than discrete ^{14}C data in summer months but lower in early spring (Yang et al. 2021).

The spectral backscattering properties of laboratory grown phytoplankton cultures vary between major taxa (Whitmire et al. 2010). The group-specific scaling factors presented in this paper are consistent with both optical theory and carbon-to-volume relationships of phytoplankton species. Experimental and modeling studies show that cells <10 um can make a disproportionately large contribution to the total backscattering signal (Dall'Olmo et al. 2009; Organelli et al. 2018), but the volume-to-carbon relationship is generally consistent across a range of taxa and sizes (Menden-Deuer and Lessard 2000). As such, our results show that b_{bp} in some populations of larger phytoplankton (nano and micro size classes) such as diatoms and dinoflagellates may require a larger scaling factor than cyanobacteria and other pico-sized
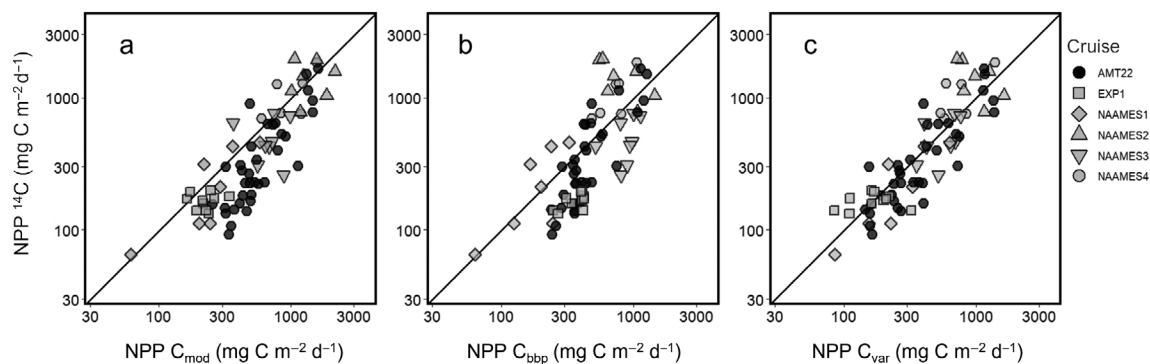
Fig. 5. NPP measured using carbon uptake (^{14}C) incubations compared with modeled estimates made using (**a**) modeled carbon ($r^2 = 0.72$, log $(y) = 1.06$ log$(x) - 0.33$, RMSE = 0.20), (**b**) phytoplankton carbon estimated following the methods of Graff et al. (2015) where the scaling factor is fixed ($r^2 = 0.57$, log$(y) = 1.10$ log$(x) - 0.46$, RMSE = 0.25) and, (**c**) phytoplankton carbon estimated with the variable scaling factor using the absorption method ($r^2 = 0.78$, log$(y) = 1.02$ log$(x) - 0.08$, RMSE = 0.18). Symbol shape indicates the cruise. Solid line in each represents the 1 : 1 line.

Table 1. Population specific daily estimates of modeled and measured depth-integrated NPP ($\int$NPP). Values are group means and standard deviation apart from $\Delta\int$NPP ($C_{b_{bp}}$–C_{var}) which is medium and range values. Units are mg C m^{-2} d^{-1}.

Population	$\int$NPP(C_{mod})	$\int$NPP ($C_{b_{bp}}$)	$\int$NPP (C_{var})	$\int$NPP (^{14}C)	$\Delta\int$NPP ($C_{b_{bp}}$–C_{var})
Cyanobacteria/haptophytes (model $n = 79$, ^{14}C $n = 48$)	485 ± 239	462 ± 225	338 ± 198	293 ± 182	$103; -181 - 539$
Diatoms/dinoflagellates (model $n = 29$, ^{14}C $n = 21$)	1155 ± 494	787 ± 346	930 ± 371	1130 ± 502	$-155; -363 - 183$
Green algae/mixed (model $n = 10$, ^{14}C $n = 4$)	373 ± 305	271 ± 195	283 ± 171	327 ± 309	$-6; -54 - 19$

phytoplankton. This relationship may not apply universally, however, and further analysis is required to improve the relationship between phytoplankton size and field measurements of b_{bp} (Qiu et al. 2021).

The two particulate absorption wavelengths identified to best estimate C_{var}, 690 and 580 nm, were somewhat surprising, but there are several plausible explanations for their selection as taxonomic indicators. Although neither wavelength is associated with absorption peaks of major diagnostic pigments, the two selected regions of the absorption spectrum could be capturing subtle differences in taxon-specific physiology (Supporting Information Fig. 4). The 690 nm wavelength is notably between the absorbance maxima of the 2nd and 1st photosystem (PS) reaction centers, which are centered at 680 and 700 nm, respectively (Falkowski & Raven, 2013). The PSII/PSI ratio varies between species, with diatoms often maintaining a higher ratio than haptophytes and green algae across a range of light intensities (Vandenhecke et al. 2015). Major taxonomic differences in the PSII/PSI ratio could therefore lead to differences in absorption in the region of spectral overlap at 690 nm and permit discrimination of communities dominated by diatoms from other groups. At 580 nm, the major pigments contributing to light absorption are phycocyanin and phycoerythrin, which are diagnostic marker pigments for red cyanobacteria, and Chl *c*, which is a dominant pigment in red algae (including diatoms, dinoflagellates, haptophytes, and others) (Chase et al. 2013; Luimstra et al. 2018). Small changes in absorption at 580 nm could therefore reflect shifts in phytoplankton community composition and the $a_{nw}(690)/a_{nw}(580)$ ratio may amplify small differences in both signals. A simpler explanation may be that 690 nm serves as a near-baseline for variation driven by the accessory pigments represented by 580 nm, but this idea does not explain why the ratios $a_{nw}(695)/a_{nw}(580)$ and $a_{nw}(700)/a_{nw}(580)$ yielded poorer correlations with $C_{mod}/b_{bp}(470)$ compared to $a_{nw}(690)/a_{nw}(580)$.

Accounting for phytoplankton group variability in the b_{bp} to C_{phyto} relationship is one step toward more reliable estimates of phytoplankton biomass but other considerations remain, such as the effects of particle composition and the non-algal contribution to scattering (Cetinić et al. 2012). The background component of the optical backscatter signal is variable and may be a notable contributor to total b_{bp} in oligotrophic waters (Bellacicco et al. 2018; Bellacicco et al. 2019). Correcting for this background component is particularly important in low biomass/low b_{bp} waters where non-algal particles impact the b_{bp} signal (Stramski et al. 2004; Organelli et al. 2018). The breakdown in relationships between C_{var} and C_{fcm} (and $C_{var} : POC$; Fig. 4) south of 35 S could be caused by an increased prevalence of pico- and nano-eukaryotes in the flow cytometry biomass estimation which relies on an empirical carbon-to-volume relationship. This result brings in a degree of uncertainty which is compounded by the difficulty in estimating size and volume for these pico- and nano-sized cells (Martinez-Vicente et al. 2013).

Further exploration into the influence of taxonomy on the scalar required for b_{bp}-derived biomass will help constrain uncertainty in measurements of phytoplankton carbon and provide more accurate model estimates of NPP. Improved estimates of biomass and NPP are also important for other rate measurements, such as net community production or carbon export, that provide key metrics of marine ecosystem health and function. The method put forward here is simple but shows that absorption-based approaches warrant further exploration to obtain taxon-specific estimates of phytoplankton carbon. Currently, most platforms that measure optical oceanographic parameters at high spatial or temporal resolution (e.g., autonomous floats, gliders or satellites) do not possess the hyperspectral capabilities required for our method. Future satellite missions (e.g., NASA's Plankton, Aerosol, Cloud, ocean Ecosystem) offer the required spectral resolution however, and optical technology is progressing at such a rate that we could soon see spectral absorption sensors incorporated into global arrays of ocean profilers. Until then, easily obtainable estimates of SF_{mod} can be used to evaluate phytoplankton group composition throughout the annual cycle using data from autonomous underwater vehicles and satellite ocean color.

References

Behrenfeld, M. J., E. Boss, D. A. Siegel, and D. M. Shea. 2005. Carbon-based ocean productivity and phytoplankton physiology from space. Global Biogeochem. Cycl. **19**: 1–14. https://doi.org/10.1002/ecm.1457

Behrenfeld, M. J., K. H. Halsey, E. S. Boss, L. Karp-Boss, A. J. Milligan, and G. Peers. 2021. Thoughts on the evolution and ecological niche of diatoms. Ecol. Monogr. **91**: e01457.

Bellacicco, M., G. Volpe, N. Briggs, V. Brando, J. Pitarch, A. Landolfi, S. Colella, S. Marullo, and R. Santoleri. 2018. Global distribution of non-algal particles from ocean color data and implications for phytoplankton biomass detection. Geophys. Res. Lett. **45**: 7672–7682. doi:10.1029/2018GL078185

Bellacicco, M., and others. 2019. Global variability of optical backscattering by non-algal particles from a biogeochemical-argo data set. Geophys. Res. Lett. **46**: 9767–9776. doi:10.1029/2019GL084078

Bolaños, L. M., and others. 2020. Small phytoplankton dominate western North Atlantic biomass. ISME J **14**: 1663–1674. doi:10.1038/s41396-020-0636-0

Boss, E., and others. 2013. The characteristics of particulate absorption, scattering and attenuation coefficients in the surface ocean; contribution of the Tara oceans expedition. Methods Oceanogr. **7**: 52–62. doi:10.1016/j.mio.2013.11.002

Boss, E. S., R. Collier, G. Larson, K. Fennel, and W. S. Pegau. 2007. Measurements of spectral optical properties and their relation to biogeochemical variables and processes in Crater Lake, Crater Lake National Park, OR. Hydrobiologia **574**: 149–159. doi:10.1007/s10750-006-2609-3

Cetinić, I., M. J. Perry, N. T. Briggs, E. Kallin, E. A. D'Asaro, and C. M. Lee. 2012. Particulate organic carbon and inherent optical properties during 2008 North Atlantic bloom experiment. J. Geophys. Res. Oceans **117**: C06028.

Chase, A., E. Boss, R. Zaneveld, A. Bricaud, H. Claustre, J. Ras, G. Dall'Olmo, and T. K. Westberry. 2013. Decomposition of in situ particulate absorption spectra. Methods Oceanogr. **7**: 110–124. doi:10.1016/j.mio.2014.02.002

Chase, A. P., S. J. Kramer, N. Haëntjens, E. S. Boss, L. Karp-Boss, M. Edmondson, and J. R. Graff. 2020. Evaluation of diagnostic pigments to estimate phytoplankton size classes. Limnol. Oceanogr. Methods **18**: 570–584. doi:10.1002/lom3.10385

Dall'Olmo, G., T. K. Westberry, M. J. Behrenfeld, E. Boss, and W. H. Slade. 2009. Direct contribution of phytoplankton-sized particles to optical backscattering in the open ocean. Biogeosci. Discuss. **6**: 291–340.

Durkin, C. A., B. A. S. Van Mooy, S. T. Dyhrman, and K. O. Buesseler. 2016. Sinking phytoplankton associated with carbon flux in the Atlantic Ocean. Limnol. Oceanogr. **61**: 1172–1187. doi:10.1002/lno.10253

Falkowski, P. G., Raven, J. A. 2013. Aquatic photosynthesis. Princeton University Press.

Finkel, Z. V., J. Beardall, K. J. Flynn, A. Quigg, T. A. V. Rees, and J. A. Raven. 2010. Phytoplankton in a changing world: Cell size and elemental stoichiometry. J. Plankton Res. **32**: 119–137.

Flombaum, P., and others. 2013. Present and future global distributions of the marine Cyanobacteria *Prochlorococcus* and *Synechococcus*. Proc. Nat. Acad. Sci. USA **110**: 9824–9829. doi:10.1073/pnas.1307701110

Fox, J., and others. 2020. Phytoplankton growth and productivity in the Western North Atlantic: Observations of regional variability from the NAAMES field campaigns. Front. Mar. Sci. **7**: 24.

Fox, J., Kramer, S. J., Graff, J. R., Behrenfeld, M. J., Boss, E., Tilstone, T., Halsey, K. H. 2022. An absorption-based approach to improved estimates of phytoplankton biomass and net primary production: Code, data and metadata. doi:10.5281/zenodo.6675894

Gardner, W. D., A. V. Mishonov, and M. J. Richardson. 2006. Global POC concentrations from in-situ and satellite data. Deep-Sea Res. II Top. Stud. Oceanogr. **53**: 718–740.

Graff, J. R., A. J. Milligan, and M. J. Behrenfeld. 2012. The measurement of phytoplankton biomass using flowcytometric sorting and elemental analysis of carbon. Limnol. Oceanogr. Methods **10**: 910–920.

Graff, J. R., and others. 2015. Analytical phytoplankton carbon measurements spanning diverse ecosystems. Deep-Sea Res. Part I Oceanogr. Res. Pap. **102**: 16–25. doi:10.1016/j.dsr.2015.04.006

Henson, S., F. Le Moigne, and S. Giering. 2019. Drivers of carbon export efficiency in the global ocean. Global Biogeochem. Cycles **33**: 891–903. doi:10.1029/2018GB006158

Heywood, J. L., M. V. Zubkov, G. A. Tarran, B. M. Fuchs, and P. M. Holligan. 2006. Prokaryoplankton standing stocks in oligotrophic gyre and equatorial provinces of the Atlantic Ocean: Evaluation of inter-annual variability. Deep Sea Res. Part II Topic. Stud. Oceanogr **53**: 1530–1547.

Kemp, A. E. S., and T. A. Villareal. 2018. The case of the diatoms and the muddled mandalas: Time to recognize diatom adaptations to stratified waters. Prog. Oceanogr. **167**: 138–149. doi:10.1016/j.pocean.2018.08.002

Kramer, S. J., D. A. Siegel, and J. R. Graff. 2020. Phytoplankton community composition determined from co-variability among phytoplankton pigments from the NAAMES field campaign. Front. Mar. Sci. **7**: 1–15.

Luimstra, V. M., J. M. Schuurmans, A. M. Verschoor, K. J. Hellingwerf, J. Huisman, and H. C. P. Matthijs. 2018. Blue light reduces photosynthetic efficiency of cyanobacteria through an imbalance between photosystems I and II. Photosyn. Res. **138**: 177–189. doi:10.1007/s11120-018-0561-5

Marañón, E., M. J. Behrenfeld, N. González, B. Mouriño, and M. V. Zubkov. 2003. High variability of primary production in oligotrophic waters of the Atlantic Ocean: Uncoupling

from phytoplankton biomass and size structure. Mar. Ecol. Prog. Ser. **257**: 1–11. doi:10.3354/meps257001

Martin, P., R. S. Lampitt, M. Jane Perry, R. Sanders, C. Lee, and E. D'Asaro. 2011. Export and mesopelagic particle flux during a North Atlantic spring diatom bloom. Deep Sea Res. Part I Oceanogr. Res. Pap. **58**: 338–349. doi:10.1016/j.dsr.2011.01.006

Martinez-Vicente, V., G. Dall'Olmo, G. Tarran, E. Boss, and S. Sathyendranath. 2013. Optical backscattering is correlated with phytoplankton carbon across the Atlantic Ocean. Geophys. Res. Lett. **40**: 1154–1158. doi:10.1002/grl.50252

Martínez-Vicente, V., and others. 2017. Intercomparison of ocean color algorithms for picophytoplankton carbon in the ocean. Front. Mar. Sci. **4**: 378.

Menden-Deuer, S., and E. J. Lessard. 2000. Carbon to volume relationships for dinoflagellates, diatoms, and other protist plankton. Limnol. Oceanogr. **45**: 569–579. doi:10.4319/lo.2000.45.3.0569

Organelli, E., G. Dall'Olmo, R. J. W. Brewin, G. A. Tarran, E. Boss, and A. Bricaud. 2018. The open-ocean missing backscattering is in the structural complexity of particles. Nat. Commun. **9**: 5439.

Qiu, G., X. Xing, E. Boss, X.-H. Yan, R. Ren, W. Xiao, and H. Wang. 2021. Relationships between optical backscattering, particulate organic carbon, and phytoplankton carbon in the oligotrophic South China Sea basin. Opt. Express **29**: 15159–15176. doi:10.1364/OE.422671

Siegel, D. A., and others. 2021. An operational overview of the EXport Processes in the Ocean from RemoTe Sensing (EXPORTS) Northeast Pacific field deployment. Element. Sci. Anthropocene **9**: 1–31.

Stramski, D., E. Boss, D. Bogucki, and K. J. Voss. 2004. The role of seawater constituents in light backscattering in the ocean. Prog. Oceanogr. **61**: 27–56. doi:10.1016/j.pocean.2004.07.001

Tarran, G. A., J. L. Heywood, and M. V. Zubkov. 2006. Latitudinal changes in the standing stocks of nano- and picoeukaryotic phytoplankton in the Atlantic Ocean. Deep Sea Res. Part II Topic. Stud. Oceanogr. **53**: 1516–1529.

Tilstone, G., T. Smyth, A. Poulton, and R. Hutson. 2009. Measured and remotely sensed estimates of primary production in the Atlantic Ocean from 1998 to 2005. Deep-Sea Res. Part II Topic. Stud. Oceanogr. **56**: 918–930. doi:10.1016/j.dsr2.2008.10.034

Vandenhecke, J. M.-R., J. Bastedo, A. M. Cockshutt, D. A. Campbell, and Y. Huot. 2015. Changes in the Rubisco to photosystem ratio dominates photoacclimation across phytoplankton taxa. Photosynth. Res. **124**: 275–291. doi:10.1007/s11120-015-0137-6

Whitmire, A. L., W. S. Pegau, L. Karp-Boss, E. Boss, and T. J. Cowles. 2010. Spectral backscattering properties of marine phytoplankton cultures. Opt. Express **18**: 15073. doi:10.1364/OE.18.015073

Xing, X., and E. Boss. 2021. Chlorophyll-based model to estimate underwater photosynthetically available radiation for modeling, in-situ, and remote-sensing applications. Geophys. Res. Lett. **48**: 1–11. doi:10.1029/2020GL092189

Yang, B., J. Fox, M. J. Behrenfeld, E. S. Boss, N. Haëntjens, K. H. Halsey, S. R. Emerson, and S. C. Doney. 2021. In situ estimates of net primary production in the Western North Atlantic with Argo profiling floats. J. Geophys. Res. Biogeosci. **126**: e2020JG006116.